JOURNAL OF GEOPHYSICAL RESEARCH, VOL. 105, NO. D3, PAGES 4019-4029, FEBRUARY 16, 2000

Global warming potential assessment for $CF_3OCF=CF_2$

Zhuangjie Li,[1] Zhining Tao,[1] Vaishali Naik,[1] David A. Good,[2] Jaron C. Hansen,[2] Gill-Ran Jeong,[1] Joseph S. Francisco,[2] Atul K. Jain,[1] and Donald J. Wuebbles[1]

Abstract. We have examined $CF_3OCF=CF_2$ regarding its reactivity toward OH radical, its infrared spectroscopic properties, its atmospheric lifetime, and its radiative forcing. From these we then determined the Global Warming Potentials (GWPs) for $CF_3OCF=CF_2$. The examination is completed using a combination of discharge flow coupled with mass spectrometer and resonance fluorescence (DF/MS/RF), Fourier transform infrared (FTIR) spectroscopy, ab initio molecular orbital calculation, and atmospheric and radiative transfer modeling. Mass spectral evidence suggests that both HF and $CF_3OCFC(O)F$ are products from the reaction of $CF_3OCF=CF_2$ with OH. The Arrhenius expression for $CF_3OCF=CF_2$ + OH is determined to be $k_1 = (6.41\pm0.82)\times10^{-11}\exp[(-868\pm40)/T]$ cm^3 molecule^{-1} s^{-1} in the temperature range of 253-348 K. The atmospheric lifetime of $CF_3OCF=CF_2$ is estimated to be less than 5 days due to the OH attack. The calculated vibrational frequencies using ab initio molecular orbital calculations are in good agreement with FTIR experimental observation for the $CF_3OCF=CF_2$ molecule. Both C-O and C-F stretching modes in the $CF_3OCF=CF_2$ contribute to prominent absorption in the atmospheric window region. The absolute adjusted radiative forcing at the tropopause due to an increase in the concentration of $CF_3OCF=CF_2$ by one part per billion by volume (ppbv) is calculated to be 0.041 W m^{-2} ppbv^{-1}. The Global Warming Potential for $CF_3OCF=CF_2$ is evaluated to be 0.004 for 100-year time horizon.

1. Introduction

Implementation of the Montreal Protocol and its amendments requires extensive evaluation of the alternatives of chlorofluorocarbons (CFCs) and bromine-containing halons to ensure that replacement compounds for CFCs and halons are environmentally acceptable. Similar analyses of greenhouse gases are necessary because of concerns about global climate change. The acceptance criterion for the alternatives has been established in terms of Ozone Depletion Potentials (ODPs) and Global Warming Potentials (GWPs) [*World Meteorological Organization (WMO),* 1995]. Thus it is important to be sure that new chemicals and existing chemicals do not have unnecessarily high ODPs and GWPs. The newly developed CFC replacement compounds without chlorine and bromine atoms are in general benign to the ozone layer, but they must meanwhile have low GWPs to be acceptable to the environment. Although the ODPs and GWPs of the alternatives are separately determined by the reactivity of the degradation intermediates/products toward stratospheric ozone and by the compounds' ability to absorb infrared radiation, they are strongly related to the atmospheric lifetime of the alternatives. Short-lived compounds are desirable to reduce both ODPs and GWPs and hence the adverse effect on the environment.

The lifetime of CFC and halon alternatives in the atmosphere is generally controlled by both photochemical and chemical removal mechanisms such as photodissociation of the replacement species and the reaction of the alternatives with other reactive species in the atmosphere such as $O(^1D)$, H, and OH [*Ravishankara et al.,* 1993]. Under tropospheric conditions the atmospheric concentrations of $O(^1D)$ and H are lower than that of OH by several orders of magnitude [*DeMore et al.,* 1997], indicating the reaction of the alternatives with OH will dominate over both $O(^1D)$ and H species. As a result, the atmospheric lifetime of most alternatives under consideration is mainly governed by photolysis and by reaction with hydroxyl radical. For many of these compounds the reaction with OH is the only important mechanism determining their atmospheric lifetimes. Thus the reaction of OH with the CFC and halon replacement compounds is critical in estmating their ODPs and GWPs.

For newly developed chemicals, knowledge about the infrared optical properties of CFC surrogate candidates and the rate of OH attack on these compounds is needed in order to model the atmospheric behavior of the substitutes so that the environmental impact of the replacements can be fully assessed. We are currently evaluating GWPs for several potential CFC alternatives by first measuring both the OH attack kinetic parameters and the infrared spectroscopic properties of the replacement compounds, then incorporating the experimental results into a radiative-chemical-transport model. The experimental measurements were made using discharge flow coupled with mass spectrometry and resonance fluorescence (DF/MS/RF) and Fourier transform infrared (FTIR) spectroscopy techniques, respectively. Ab initio calculations were employed in the examinations to help understand and interpret the experimental data. In this paper we present GWP evaluation of HFE-216 ($CF_3OCF=CF_2$), a potential CFC replacement compound for dry etching processing in microelectronic industry [*Yoshida,* 1998], by carrying out the above procedure.

2. Experimental Methods

2.1. Rate Constant Measurement for the Reaction of $CF_3OCF=CF_2$ With OH

The DF/MS/RF equipment for the kinetics study of OH reaction with $CF_3OCF=CF_2$

[1]Department of Atmospheric Sciences, University of Illinois at Urbana-Champaign.

[2]Department of Chemistry and Department of Earth and Atmospheric Sciences, Purdue University, West Lafayette, Indiana.

Paper number 1999JD900943.
0148-0227/00/1999JD900943$09.00

(R1) $CF_3OCF=CF_2 + OH \rightarrow$ products

is shown in Figure 1. Note that the drawing only illustrates the relative position of the instrument, not the actual size or distance of the instrumental elements. The DF/MS system in present study has been described previously [*Li et al.*, 1997; *Li*, 1999], and is only briefly discussed here. The reactor consisted of an 80-cm-long, 5.08-cm-ID Pyrex tube coated with halocarbon wax to reduce OH wall losses. The reactor temperature could be varied between 250 and 350 K by circulation of cooled methanol or heated ethylene glycol through an outer Pyrex jacket. The temperature of the circulating fluids was measured by a thermocouple located in the liquid reservoir and controlled to a precision of 0.2 K by use of a thermostatted heat exchanger. The vacuum chamber for the discharge flow-modulated molecular beam mass spectrometer was a two-stage differentially pumped vacuum system utilizing two 6-inch diffusion pumps with liquid nitrogen baffles, and the ultimate vacuum in the second stage was $< 5x10^{-10}$ torr ($6.7x10^{-8}$ Pa). A 125 cfm mechanical pump (Edwards Model E2M175) maintained the steady state pressure in the reactor at normally 1 torr (133 Pa). Helium was used as the main buffer gas and was admitted through a sidearm located upstream of the reactor. The resulting reactor flow velocities ranged between 800 and 2000 cm s^{-1}; the corresponding gaseous residence times within the reactor were between 100 and 40 ms. A removable liquid nitrogen trap was placed downstream of the reactor in order to protect the vacuum pump from corrosive reactants and products.

OH radicals were produced either by reaction of H with NO_2:

(R2) $H + NO_2 \rightarrow OH + NO$
$k_2 = 1.3 \times 10^{-10}$ cm^3 molecule^{-1} s^{-1}

or by reaction of F with H_2O [*DeMore et al.*, 1997]:

(R3) $F + H_2O \rightarrow OH + HF$
$k_3 = 1.4 \times 10^{-11}$ cm^3 molecule^{-1} s^{-1}

Atomic H and F were produced by microwave discharge of H_2 and F_2, respectively. The OH radical was detected by resonance fluorescence [*Wine et al.*, 1979; *Leu*, 1979; *Ravishankara et al.*, 1981]. The resonance lamp for the radiation of OH in the $A^2\Sigma \rightarrow X^2\Pi$ band at 309 nm was built by microwave discharging ~3 torr (400 Pa) of H_2O/He mixture in a quartz tube [*Leu*, 1979; *Leu and Smith*, 1981, 1982]. The OH resonance fluorescence signal was monitored using a photomultiplier tube (HAMAMATSU HC124-02 with R269 photomultiplier tube assembly) that was perpendicular to the resonance radiation. A UV enhanced

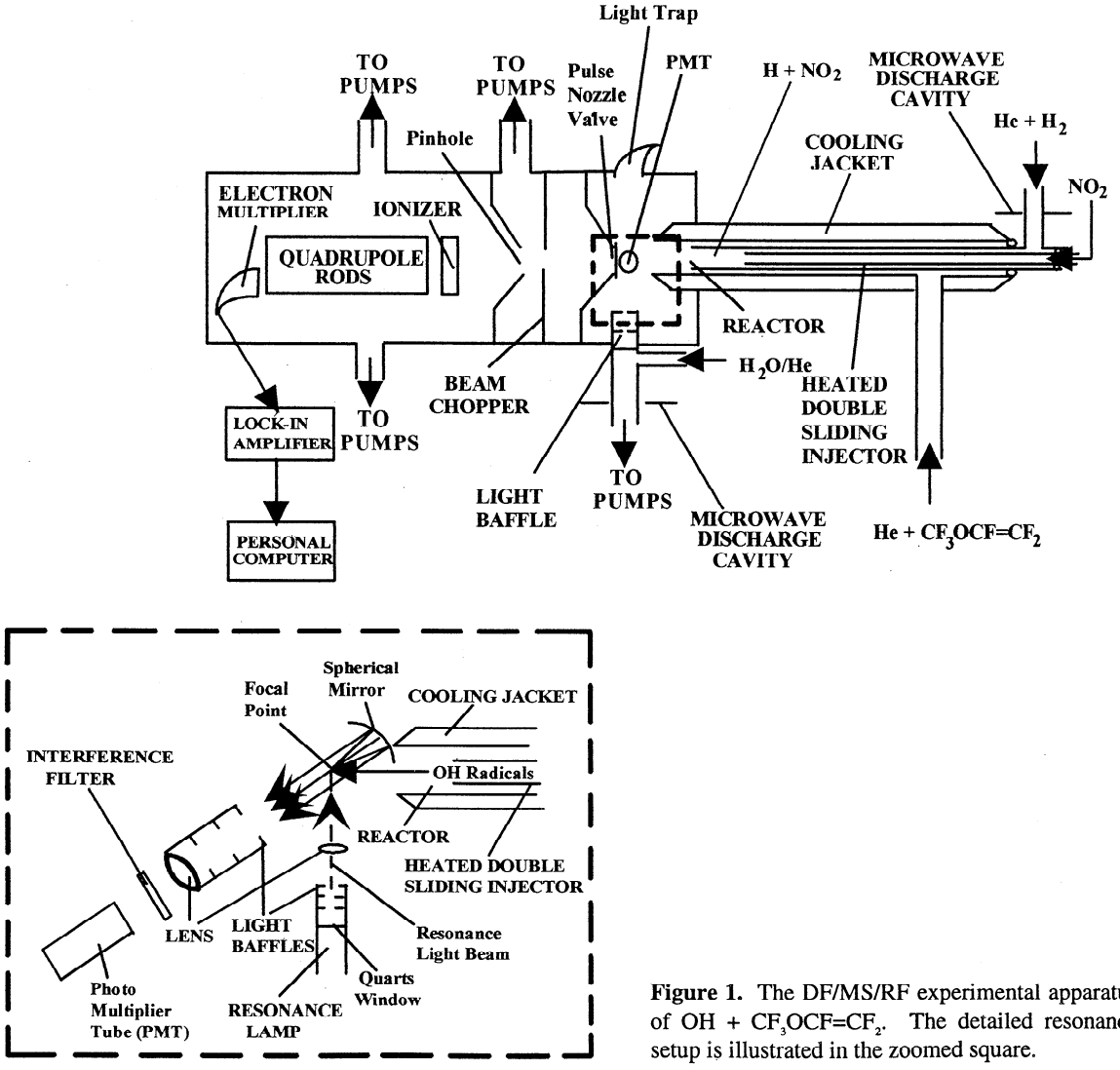

Figure 1. The DF/MS/RF experimental apparatus for the study of OH + $CF_3OCF=CF_2$. The detailed resonance fluorescence setup is illustrated in the zoomed square.

spherical mirror (1/f = 50 mm, Edmund Scientific Company) was placed in the OH fluorescence zone in alignment with the photomultiplier tube to increase the OH fluorescence photon collection. The OH fluorescence signals were sent to a lock-in amplifier (Model SR510, Stanford Research Systems, Inc.) that was referenced to a chopper frequency chopping the resonance radiation, and the signals were then digitized (Analog Devices RTI/815) and recorded on the microcomputer. Light baffles were placed in both pathways of resonance and fluorescence radiation to reduce the scattered light. It was found that the scattered light was greatly reduced with the use of the light baffles. The proportionality constant relating fluorescence signal to OH concentration was determined by titration of OH by Br_2 [*DeMore et al.*, 1997]:

(R4) $$OH + Br_2 \rightarrow HOBr + Br$$
$$k_4 = 4.2 \times 10^{-11} \text{ cm}^3 \text{ molecule}^{-1} \text{ s}^{-1}$$

such that $[OH] = [Br_2]_{consumed}$. Possible products from reaction (R1) were detected and characterized mass spectroscopically. The rate constant for reaction (R1) was then measured. A general procedure of acquiring DF/MS kinetics information for reactions involving radical species has been described previously [*Li et al.*, 1995], and kinetic parameter measurements using the DF/MS/RF technique shared the same theory as that of DF/MS. Briefly, the pseudo-first-order rate constant k' for reaction (R1) in which $[CF_3OCF=CF_2]_0 >> [OH]_0$ is defined by [*Howard*, 1979; *Mellouki et al.*, 1995]

$$-v\frac{d[OH]}{dz} = k'[OH] \quad (1)$$

where $k' = k_1[CF_3OCF=CF_2]_0 + k_0$, v is the carrier gas flow velocity, z is the injector position, k_1 is the bimolecular rate constant for reaction (R1), and k_0 is the first-order OH disappearance rate constant in absence of $CF_3OCF=CF_2$. Under our experimental conditions, $k_0 \leq 15$ s^{-1}. The measured pseudo-first-order rate constants were corrected for both axial and radial diffusions [*Howard*, 1979; *Brown*, 1978], and the corrected pseudo-first-order rate constant is signified as k'_{corr}. By varying the initial $CF_3OCF=CF_2$ concentration, different decay rates were collected. When the corrected pseudo-first-order decay rate was plotted as a function of $[CF_3OCF=CF_2]_0$, the slope of the fitted straight line yielded the binary rate constant for reaction (R1) at the temperature of the reactor. Repeating the above procedure at different temperatures allowed the measurement of the rate constant as a function of temperature. Activation energy for reaction (R1) was then determined by measuring the slope of the fitted straight line from the plot of $\ln k_1$ versus $1/T$, where T stands for temperature in kelvins.

In order to obtain reliable kinetic parameter for reaction (R1) it was necessary to check the experimental apparatus for accuracy. We used both reaction (R4) and the OH self-reaction

(R5) $$OH + OH \rightarrow H_2O + O$$
$$k_5 = 1.9 \times 10^{-12} \text{ cm}^3 \text{ molecule}^{-1} \text{ s}^{-1}$$

to calibrate our kinetic apparatus. This was done by measuring the rate constant for reactions (R4) and (R5) at 298 K with our apparatus, in which the initial concentrations of Br_2 and OH were $(3.62\text{-}10.12)\times10^{12}$ and $(4.43\text{-}6.38)\times10^{11}$ molecule cm^{-3} for reaction (R4), and the initial concentration of OH was $(1.12\text{-}1.77)\times10^{13}$ molecule cm^{-3} for reaction (R5), respectively. A rate constant of $(4.05\pm0.64)\times10^{-11}$ cm^3 molecule^{-1} s^{-1} and $(1.94\pm0.30)\times10^{-12}$ cm^3 molecule^{-1} s^{-1} was obtained for reactions (R4) and (R5), respectively. These rate constants were in good agreement with the recommended values by the NASA chemical kinetic data evaluation panel, suggesting that our experimental setup was functioning properly and ready for kinetic study of reaction (R1).

2.2. FTIR Cross Section Determination of $CF_3OCF=CF_2$

A Mathanson Galaxy 7020 spectrometer with 1 cm^{-1} resolution was employed for the $CF_3OCF=CF_2$ IR measurements. The $CF_3OCF=CF_2$ samples were purified by several freeze-pump-thaw cycles prior to its infrared cross-section measurement. After degassing at liquid N_2 temperature followed by pumping for approximately 0.5 hours to remove volatile impurities, preliminary IR spectra of the samples were taken and compared with previously published IR spectra to identify possible impurities. Samples of $CF_3OCF=CF_2$ were then transferred to a 18.0 cm Teflon cell with NaCl windows for IR measurements. The pressure within the cell was measured by calibrated MKS capacitance manometers using a 100–torr (1.33×10^4 Pa) sensor. Spectra were measured at room temperature (296 ± 2 K) for several pressures of $CF_3OCF=CF_2$ between 0.24 torr (32 Pa) and 1.5 torr (200 Pa).

For the IR measurements the integrated absorbance values were obtained by using an algorithm available on the Mathanson Galaxy 7020 computer-aided operating system. Several scans of the background (i.e., the empty cell) were averaged to generate a baseline profile. As a result, the average absolute absorbance values of the sample were calculated by baseline subtraction. Also, each data point in the Beer's law fit represents an average of three separate measurements with 64 scans for each measurement.

Beer's law was obeyed over the pressure ranges of this study for the IR measurements of $CF_3OCF=CF_2$. The errors in the determination of the IR cross sections originate from the uncertainty in the absolute absorbance values, optical path length, and pressure of the gas sample. The IR absorbance cross sections in this work were back-calculated from the slope of the Beer's law plots, and the reported uncertainties represent two standard deviations from the least squares analysis.

The gases used in this work were obtained mainly from S. J. Smith Welding Supply: He, 99.999%; H_2, 99.999%; F_2, 5% in Helium, and NO_2, 99.5%. Br_2, > 99% was obtained from Fisher Scientific. $CF_3OCF=CF_2$, > 99.9% was purchased from OAKWOOD PRODUCTS, INC.

3. Theoretical Approaches

3.1. Ab Initio Computations

Since $CF_3OCF=CF_2$ is a complex polyatomic species, it is difficult to experimentally determine the detailed structure of this molecule. Theoretical study of this molecule, on the other hand, can provide the structural information of this species, which is helpful in understanding the physical and chemical properties of $CF_3OCF=CF_2$. Ab initio molecular orbital calculations were performed with the GAUSSIAN 94 series of programs [*Frisch et al.*, 1995] using the 6-31G(d) basis set. All geometries were optimized to better than 0.001Å for bond distance and 0.1° bond angles using Schlegel's method [*Schlegel*, 1982] with a convergence of at least 10^{-9} on the density matrix; the residual rms forces were always less than the 10^{-4} a.u. Equilibrium geometries were also fully optimized with the Becke's nonlocal three-

parameter exchange with the Lee-Yang-Parr correctional functional (B3LYP) method [*Lee et al.*, 1988; *Becke*, 1993]. Vibrational frequencies and intensities were computed using analytical second derivatives at the B3LYP level of theory.

3.2. Global Atmospheric Model for Atmospheric Lifetime Calculation

The UIUC two-dimensional chemical-radiative-transport model of the global atmosphere used for atmospheric lifetime calculation is a coupled numerical model that includes explicit description of both atmospheric physical and chemical processes needed to understand the distribution of a chemical and its effects on atmospheric chemistry. The model has state-of-the-art representation of tropospheric and stratospheric processes. This zonally averaged model determines the atmospheric distributions of 66 chemically active atmospheric trace constituents. The model incorporates the important species and relevant chemistry to evaluate the spatially and temporally varying concentrations in the distributions of the O_x, HO_x, NO_y, Cl_y, Br_y, and CH_xO_y constituents affecting the global atmosphere. Transport of species in the model is self-consistently calculated using the predicted model ozone and seasonally varying climatological temperatures. Effects of heterogeneous chemistry on sulfate aerosols and polar stratospheric clouds are included in the model. Both thermal and photolytic reactions are incorporated in the model to represent the chemistry of all the species included. Thermal reaction rate constants and UV absorption cross sections are taken from the NASA panel recommendations provided by *DeMore et al.* [1997]. The removal of $CF_3OCF=CF_2$ via reaction with hydroxyl radicals is included in the model using the kinetic data collected for reaction (R1) in the present study. Two cases are considered for the emission of $CF_3OCF=CF_2$ in the model. In the first case, $CF_3OCF=CF_2$ is emitted globally, and in the second case it is emitted only in the Northern Hemisphere midlatitudes (representative of the major industrial areas). In both cases the model is run to steady state to examine the resulting effects on ozone.

The atmospheric lifetime of $CF_3OCF=CF_2$ is determined as the ratio of its abundance to its loss rate in the atmosphere. The loss rate and abundance are determined by its reaction with OH, as it is the only $CF_3OCF=CF_2$ removal reaction included in the model. The lifetime due to reaction with OH radicals is given by the following equation:

$$\tau_{CF_3OCF=CF_2} = (k_1[OH])^{-1} \quad (2)$$

where k_1 represents the rate constant for the reaction of $CF_3OCF=CF_2$ with OH radicals and [OH] represents the global average atmospheric concentration of OH. The global distributions of OH cannot readily be measured directly, as it has small atmospheric concentrations and is highly variable, responding instantly to changes in a variety of parameters including solar flux, and temperature, plus concentrations of O_3, H_2O, NO_x, CO, and CH_4. Uncertainties in the model-derived OH distribution are tested, at least in an averaged sense, by comparison with the measured amounts of gases removed primarily by tropospheric OH. Presently, methyl chloroform (CH_3CCl_3) is the primary gas used to estimate the globally averaged tropospheric OH [*Intergovernmental Panel on Climate Change (IPCC)*, 1995, 1996; *Prinn et al.*, 1995]. The tropospheric lifetime of CH_3CCl_3 used relative to reaction with tropospheric OH is 5.7 years [*Wuebbles et al.*, 1998]. Lifetime of $CF_3OCF=CF_2$ has also been determined by an alternate method that involves scaling the ratio of OH reaction rate constant of methyl chloroform to that of $CF_3OCF=CF_2$ at 277 K. This simple method was developed by *Prather and Spivakovsky* [1990] to determine the lifetime of compounds that react primarily with OH in the atmosphere.

3.3. Radiative Transfer Model for Radiative Forcing and GWPs Evaluation of $CF_3OCF=CF_2$

The concept of radiative forcing [*IPCC*, 1990, 1995, 1996] gives an estimate of the potential effect on climate due to changes in greenhouse gas concentration. The definition of radiative forcing adopted by *IPCC* [1990, 1995, 1996] has been the perturbation to the net irradiance (in W m^{-2}) at the tropopause after allowing for stratospheric temperatures to readjust to radiative equilibrium, but with the surface and tropospheric temperature and atmospheric moisture field held fixed. It is expressed in terms of the radiative forcing per unit concentration change in the atmosphere. If no change in stratospheric temperature is accounted for, the greenhouse gas radiative forcing is referred to as instantaneous radiative forcing. Once radiative forcing is evaluated, we then derive the Global Warming Potential for the compound.

Both the absolute instantaneous and adjusted radiative forcings due to $CF_3OCF=CF_2$ were evaluated using the University of Illinois at Urbana-Champaign (UIUC) radiative transfer model. This model accounts for the solar and infrared radiative effects of H_2O, CO_2, O_3, along with the effects of other gases (e.g., CH_4, N_2O, CFCs) and aerosols. It has been used in studies of the radiative forcing of trace gases and aerosols, tropospheric and stratospheric simulations, as well as studies comparing simulated long-wave radiances in restricted band (such as 10 μm water vapor window) with observations [*Briegleb*, 1992a, b; *Kiehl and Briegleb*, 1993]. The changes in the total radiative flux caused by increase in trace gases predicted by the model agree well with detailed line-by-line calculations. This model has also been used to estimate the radiative forcings for some fluoroethers [*Good et al.*, 1998].

The radiative transfer model uses the Community Climate Model, Version 2 (CCM2) short wave radiation code and long wave band model. The long wave radiation scheme used in this model is based on the Malkmus random band model of *Briegleb* [1992a]. A spectral width of 100 cm^{-1} is used to compute wide-band absorptivities and emissivities in the range 0-3000 cm^{-1}. Cloudy-sky conditions are incorporated by using data from *Christidi et al.* [1997]. A global and annual mean atmosphere (GAM) is used for radiative forcing calculations, which has also been taken from the same source. This atmosphere contains vertical profiles of pressure, temperature, H_2O, and O_3, at 16 levels. CO_2, CH_4, and N_2O mixing ratios are assumed to be constant throughout the atmosphere with a quantity of 364, 1.75, and 0.28 ppmv, respectively. The spectroscopic data for the five gases H_2O, O_3, CO_2, CH_4, and N_2O are from the HITRAN-86 database [*Rothman et al.*, 1987].

Many studies [*Pinnock et al.*, 1995; *Christidis et al.*, 1997; *WMO*, 1998] have pointed out that the assumption of a constant vertical profile may not be realistic for gases that have lifetimes shorter than the timescale of vertical mixing processes. Hence we have considered both a constant and a decaying vertical profile for the evaluation of radiative forcing due to $CF_3OCF=CF_2$. The falling-off vertical profile for the mixing ratio of $CF_3OCF=CF_2$ is derived from the UIUC two-dimensional chemical-radiative-

transport model [*Wuebbles et al.*, 1991; *Patten et al.*, 1994; *Rahmes et al.*, 1999] of the global atmosphere and interpolated to the pressure levels in GAM.

Global Warming Potentials (GWPs) is an important concept that is used to estimate the relative impact of emission of a fixed amount of one greenhouse gas compared to another for globally averaged radiative forcing of the climate system over a specified time scale. GWPs are generally expressed as the time-integrated radiative forcing from the instantaneous release of a kilogram of a gas expressed relative to that of a kilogram of the reference gas, CO_2 [*IPCC*, 1990, 1992, 1995, 1996]

$$\mathrm{GWP}_x(t') = \frac{\int_0^{t'} F_x \exp\left(-t/\tau_x\right) dt}{\int_0^{t'} F_{CO_2} R(t) dt} \qquad (3)$$

where F_x and F_{CO_2} are the radiative forcing per unit mass of species of x *and* CO_2,, τ_x is the atmospheric lifetimes of species x, and $R(t)$ represents the response function which describes the decay of an instantaneous pulse of CO_2. The numerator and the denominator represent the Absolute Global Warming Potential (AGWP) of species x and CO_2, respectively. In this study, the latest values of CO_2 AGWP from *WMO* [1998] were used to evaluate the GWPs for $CF_3OCF=CF_2$.

4. Results and Discussion

4.1. Products and Kinetic Study of Reaction of $CF_3OCF=CF_2$ With OH

There were two tasks in the experimental examination of reaction (R1). The first one was to investigate the reaction mechanism by probing the products from reaction (R1). The second task was to measure the rate constant of reaction (R1). In searching for products from reaction (R1), when (3~5) x 10^{13} molecule cm^{-3} of $CF_3OCF=CF_2$ was added into the reactor containing ~2x10^{12} molecule cm^{-3} of OH produced using reaction (R2), a signal at m/*e*=20 was observed, suggesting that HF was formed in the reactor.

The HF appeared to be the product from reaction (R1) on the basis of several controlled experiments, in which little HF was observed in the absence of either OH or $CF_3OCF=CF_2$. The reaction of $CF_3OCF=CF_2$ with atomic hydrogen could be one possible chemical process in the reactor that contributed to the formation of HF:

(R6) $\quad CF_3OCF=CF_2 + H \rightarrow HF + \text{other product(s)}$

In a controlled experiment, reaction (R6) was allowed to take place in the reactor by having the $CF_3OCF=CF_2$ in contact only with the H atoms generated in the sliding injector. Very little HF was detected from the reaction (R6). However, when NO_2 was introduced into the double sliding injector to convert the hydrogen atoms into OH radicals, the HF was observed, confirming that the HF was a product from reaction (R1). The signals at m/*e*=20 were at least 2 times greater than the background. It was also noticed that the amount of HF increased with both the OH concentration and the contact time between the $CF_3OCF=CF_2$ and the OH radicals.

There were two possible mechanisms to account for the production of HF from reaction (R1): (1) reaction (R1) proceeded through a process involving an intermediate species, probably in the form of adduct, followed by rearrangement and dissociation of the intermediate, namely,

(R1a) $\quad CF_3OCF=CF_2 + OH \leftrightarrow CF_3OCF(OH)CF_2$

(R1b) $\quad CF_3OCF(OH)CF_2 \rightarrow HF + CF_3OCFC(O)F$ or $CF_3OC(O)CF_2$.

(2) Reaction (R1) took place through a four-center transition state leading to the simultaneous rupture of a C-F bond and an O-H bond, and the formation of a C-O bond and an H-F bond:

(R1c) $\quad CF_3OCF=CF_2 + OH \rightarrow [CF_3OCFC(O\cdots H)\cdots F]^{\ddagger} \rightarrow HF + CF_3OCFC(O)F$ (F on the C bearing the CF$_3$O group)

(R1d) $\quad CF_3OCF=CF_2 + OH \rightarrow [CF_3OC(O\cdots H)\cdots FCF_2]^{\ddagger} \rightarrow HF + CF_3OC(O)CF_2$.

Nevertheless, we were unable to observe the parent ion of either $CF_3OCF(OH)CF_2$ (m/e=183) or $CF_3OCFC(O)F$ [or $CF_3OC(O)CF_2$] (m/*e*=163) species. Thus it was unclear at this moment which reaction pathway reaction (R1) followed since our instruments did not have the capability to make such a distinction. However, as we will see in later discussion, our kinetic results from the temperature-dependent study of the reaction (R1) suggest that the reaction might prefer the mechanism of reaction (R1a) followed by (R1b).

It would be interesting to examine which of the doubly bonded carbon atoms the OH radical was adding to. This can be inferred by examining the possible ion species that was fragmented from large product species. In the products searching experiments we detected a signal at m/*e*=47, assigned to FCO, which was at least 40% above the background due to the fragmentation of the $CF_3OCF=CF_2$. Even though the products were not quantified, it was found that the FCO signals, like the HF signals, clearly increased with contact time between OH and $CF_3OCF=CF_2$. This observation suggests that one of the products from reaction (R1) would have an FCO-like structural feature. The $CF_3OCFC(O)F$ radical could be such a candidate, since either the further dissociation or the fragmentation of this species in the ionization zone of the mass spectrometer would give rise to the detection of the FCO signal. Moreover, it was conceivable that the CF_3O- group was much greater in volume than the F atom, and it would provide more stereo hindrance for the addition of the OH radical onto the carbon atom connecting the CF_3O- group than that bonding only to fluorine atoms. As a result, the OH radical tended to attack the carbon atom connecting two fluorine atoms. On the basis of our observations and analysis, we conclude that reaction (R1) leads to production of HF and $CF_3OCFC(O)F$. The reaction mechanism for reaction (R1) thus seems to be complex, and our observation of both HF and $CF_3OCFC(O)F$ as products from reaction (R1) offers valuable but insufficient information for the complete understanding of the reaction pathway of this reaction. In a kinetic study of OH reaction with perfluoropropene ($CF_3CF=CF_2$), *McIlroy and Tully* [1993] used an OH + hydrogenated unsaturate reaction model to analyze their experimental data. The model considered a general reaction

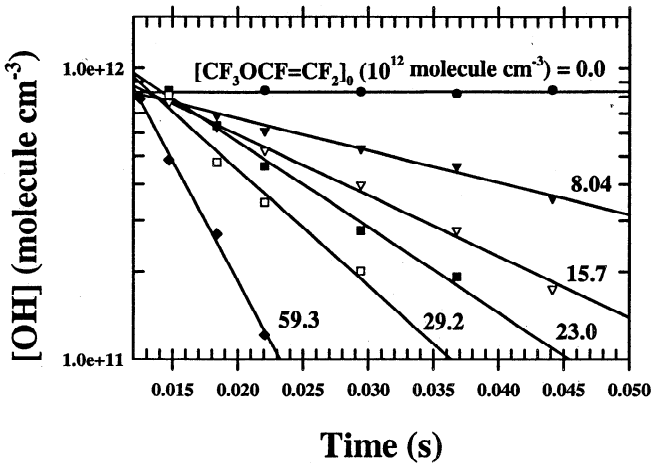

Figure 2. Typical OH decay at 298 K as a function of time in the presence of different $CF_3OCF=CF_2$ initial concentrations. The OH radicals were produced from F + H_2O. The temperature of the reactor was 298 K, and the pressure was 1.0 torr (133 Pa). The flow velocity of this run was 1360 cm s^{-1}.

mechanism considering three reaction pathways: (1) formation of reversible adduct, (2) adduct decomposition, and (3) direct hydrogen-atom abstraction. They concluded that the fluorination of the unsaturated reactants significantly complicates the reaction mechanism due to the electron-drawing properties of fluorine. This complication might have contributed to the inconclusive reaction mechanism in the present study for the reaction (R1).

Figures 2 and 3 show the experimental data for kinetic study of reaction (R1), in which Figure 2 displays the decay of OH as a function of reaction time in the presence of different $CF_3OCF=CF_2$ initial concentrations. In the present study of reaction (R1), the initial concentration of OH and $CF_3OCF=CF_2$ were (5-8) x 10^{11} and (4-60) x 10^{12} molecule cm^{-3}, respectively, thus $[CF_3OCF=CF_2]_0/[OH]_0 > 5$. It can be seen from Figure 2 that

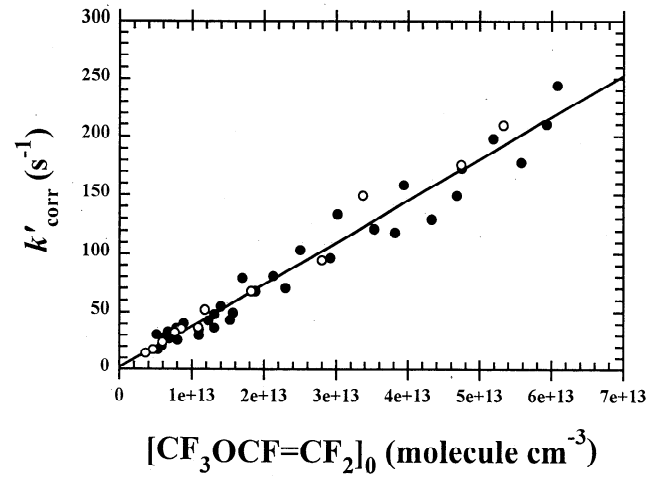

Figure 3. Pseudo-first-order decay rate (corrected for both axial and radial diffusion) of the OH radical as a function of $[CF_3OCF=CF_2]_0$ at 298 K. The data points in solid circle were taken using F + H_2O as the OH source, and those in open circle were taken using H + NO_2 as the OH source. Data were collected with a total pressure of 1.0 torr (133 Pa) in the reactor, and the flow rate was 1300~1400 cm s^{-1}.

Table 1. Rate Constant k for the Reaction of $CF_3OCF=CF_2$ With OH Radical

Temperature, K	k x 10^{12} cm^3 molecule^{-1} s^{-1}
253	2.07±0.24 (16)
277	2.76±0.39 (18)
298	3.58±0.42 (47)
323	4.36±0.90 (10)
348	5.26±0.90 (11)

The errors are taken as 2σ which takes into account the scatter of the data and the uncertainty of experimental parameters. The numbers in parentheses stand for the number of measurements taken at corresponding temperature.

the OH decay appeared to follow the pseudo-first-order behavior, and within a reaction time domain of about 50 ms, the OH decayed faster with increase of the initial $CF_3OCF=CF_2$ quantity in the reactor. The slope of the OH decay thus yielded a pseudo-first order decay rate at corresponding $[CF_3OCF=CF_2]_0$. Figure 3 shows the pseudo-first-order decay rate as a function of the $CF_3OCF=CF_2$ initial concentration. Our data indicate that at 298 K the pseudo-first-order decay rate for the reaction (R1) varied from 10 to 240 s^{-1} when the initial $CF_3OCF=CF_2$ concentrations were altered in a range of (4~60) x 10^{12} molecule cm^{-3}. Notice that consistent decay rates were obtained using both reactions (R2) and (R3) as the OH sources. The bimolecular rate constant for the reaction (R1) was then determined from the slope of the fitted straight line through all experimental data points, which gives k_1 = (3.58±0.42) x 10^{-12} cm^3 molecule^{-1} s^{-1} at 298 K. The quoted uncertainty corresponded to 2σ and reflects the scatter of the data and the uncertainties of the experimental parameters such as temperature, flow rate, and pressure.

It is worthwhile to compare reactivity of $CH_3OCH=CH_2$ and $CF_3OCF=CF_2$ toward OH to see the effect of fluorination of $CH_3OCH=CH_2$ on the OH rate constant. The rate constant for the reaction of the OH radical with vinyl methyl ether ($CH_3OCH=CH_2$) was measured to be (3.35±0.34) x 10^{-11} cm^3 molecule^{-1} s^{-1} at room temperature [*Perry et al.*, 1977], which is about 10 times greater than that of reaction (R1). This indicates

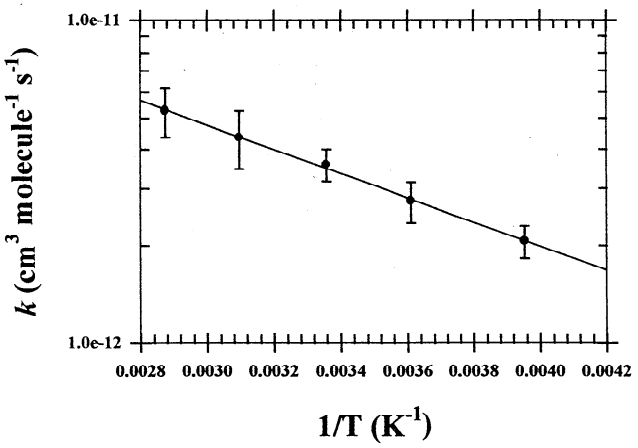

Figure 4. Arrhenius plot of log$k$ against 1/T for the reaction of $CF_3OCF=CF_2$ with OH.

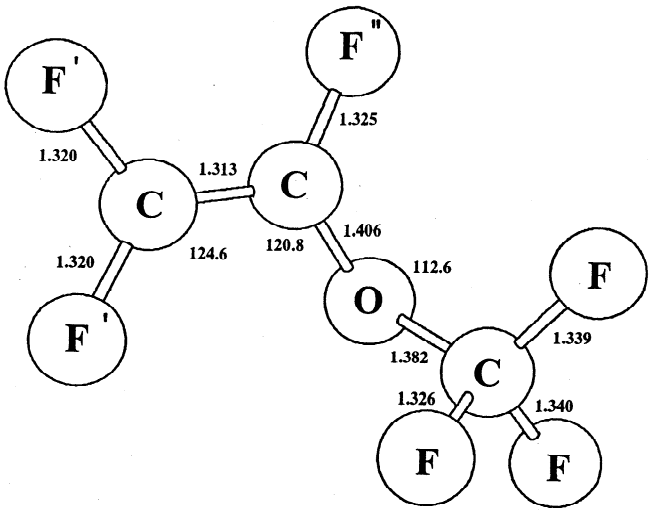

Figure 5. Structure of the $CF_3OCF=CF_2$ molecule. Structural parameters are from the B3LYP/6-31G(d) calculation.

that the substitution of hydrogen atoms with fluorine atoms in the $CH_3OCH=CH_2$ significantly reduces the reactivity of this ether molecule toward the OH radicals. Moreover, the rate constant for the reaction of OH with perfluoropropene ($CF_3CF=CF_2$) was measured at 298 K to be (2.26±0.12) x 10^{-12} cm^3 $molecule^{-1}$ s^{-1} by *McIlroy and Tully* [1993] and (2.17±0.01) x 10^{-12} cm^3 $molecule^{-1}$ s^{-1} by *Orkin et al.* [1997]. The rate constant measured at 298 K for reaction (R1) in the present work is comparable to both values.

The dependence of the rate constant on temperature for reaction (R1) in the temperature range of 253-348 K was examined in present work with an interval of about 20 K. Rate constant for each temperature was obtained from the linear least squares fit through the OH decay data at corresponding temperature, and the results are summarized in Table 1. As seen in the Table 1, our experimental data indicate that the rate constant for the reaction of $CF_3OCF=CF_2$ with OH increases with temperature. Figure 4 displays the data in Table 1 in Arrhenius form. A linear least squares analysis of the data in the Figure 4 yields the Arrhenius expression

$$k_1 = (6.41\pm0.82)\times10^{-11} \exp[-(868\pm40)/T] \text{ cm}^3 \text{ molecule}^{-1} \text{ s}^{-1}$$

for reaction (R1), where the errors in both the A factor and the activation energy are taken as 2σ. We notice that the A factor in the Arrhenius expression is substantially higher than that of typical OH reaction with unsaturated halocarbons such as C_2Cl_4 [*Chang and Kaufman*, 1977], and this high A factor might be associated with the rapid formation of the adduct described by reaction (R1a). The positive temperature dependence of the rate constant for the reaction (R1) has not been understood. A similar behavior was also reported for the reaction of OH with C_2Cl_4 [*Chang and Kaufman*, 1977]. In our case the positive temperature dependence of the rate constant for the reaction (R1) could imply a reaction mechanism including a small activation energy, such as that of reaction (R1b) discussed previously.

4.2. Structure and Vibrational Spectrum of $CF_3OCF=CF_2$

The optimized geometry for $CF_3OCF=CF_2$ is shown in Figure 5. Significant structural parameters obtained from the B3LYP/6-31G(d) calculation are also contained in Figure 5. The CF bond distance on the CF_3 group seemed reasonably well predicted when compared to CF bond distance for CF_3-containing compounds. For example, the CF bond distances in the CF_3 group of $CF_3C(O)F$ was measured to be 1.330 ± 0.020Å [*Boulet*, 1964].

Table 2. Vibrational Frequencies and Intensities for $CF_3OCF=CF_2$

Mode Number	Approximate Mode Description	Frequency, cm^{-1}		Intensity	
		B3LYP/ 6-31G(d)	Experimental	B3LYP/ 6-31G(d)	Experimental[a]
1	CC stretch	1896	1842	17	W
2	CF' asymmetric stretch	1373	1342	198	S
3	CF" stretch	1328		168	
4	CF (CF_3 group) stretch	1325	1306	421	
5	CF (CF_3 group) asymmetric stretch	1251	1231	329	S
6	CO asymmetric stretch	1204	1195	383	VS
7	CF' symmetric stretch	1190	1180	422	S
8	CF (CF_3 group) symmetric. Stretch	913	908	14	W
9	CO symmetric stretch	819	814	5	W
10	COC bend	696		5	
11	CF_2' bend	631		7	
12	CF_2' rock	624		7	
13	CF_2' wag	545		3	
14	CF_2 scissors	540		1	
15	CF_2 rock	519		2	
16	FCO deformation	454		1	
17	OCC bend	428		2	
18	CF_2 twist	359		0.4	
19	F"CO deformation	334		1	
20	CF_2' scissors	205		3	
21	F'CCF" twist	186		1	
22	FCOC torsion	112		1	
23	F"COC torsion	61		0.003	
24	F'CCO torsion	26		0.01	

[a]W, weak; S, strong; VS, very strong.

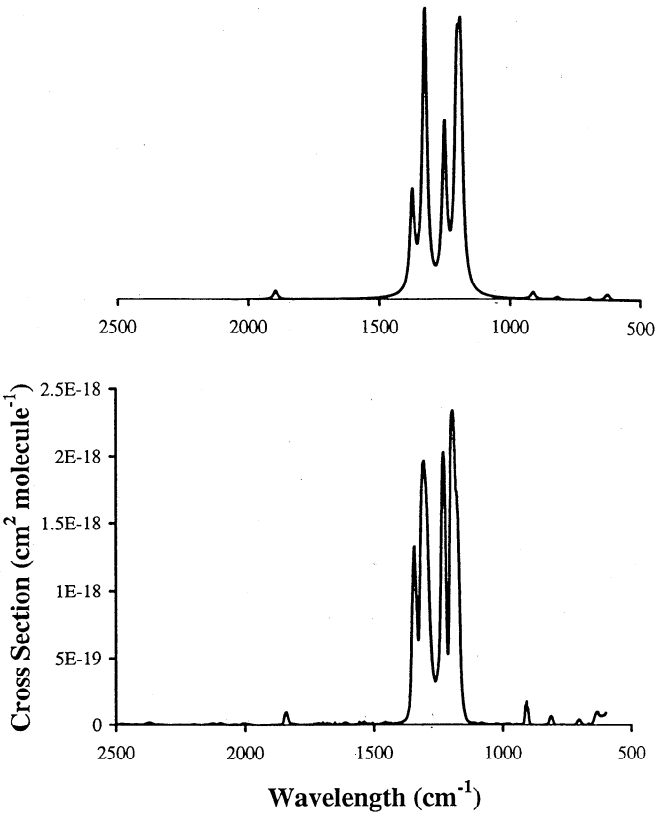

Figure 6. (top) Simulated and (bottom) experimental IR spectrum of $CF_3OCF=CF_2$ from 2500-500 cm^{-1}.

Our predictions of 1.339Å and 1.340Å were also reasonable when compared to the experimental bond length of 1.410Å measured in dimethyl ether [*Blukis et al.*, 1963]. In dimethyl ether the two CO bond lengths were equivalent, while in $CF_3OCF=CF_2$, they were not. This is because the CF_3 group acts to stabilize the CO bond through hyperconjugation effects.

In Table 2 we report the vibrational assignment of $CF_3OCF=CF_2$. The structural model used to describe this molecule was C_1 symmetry. All twenty-four fundamental modes were allowed both in IR and Raman spectrum. A normal coordinate analysis was carved out to obtain a more complete description of the molecular motion in the fundamental vibration of $CF_3OCF=CF_2$. The vibrational frequencies and assignments were made from calculation at the B3LYP/6–31G(d) level of theory. The measured IR spectrum and the simulated IR spectrum from the B3LYP/6-31G(d) calculation are provided in Figure 6. The infrared spectra of $CF_3OCF=CF_2$ were measured between 3000 and 500 cm^{-1}. As a further test of the reliability of the calculations, we simulated the infrared spectrum from the ab initio frequencies. The simulated spectrum was generated using the calculated frequencies as the mean of a Lorentzian distribution with a full width at half maximum (FWHM) of 16 cm^{-1}. The Lorentzian is given by the following expression:

$$\frac{1}{\pi}\frac{\Delta x/2}{(\Delta x/2)^2+(x-u)^2} \tag{4}$$

where u is the mean or central frequency and Δx is the FWHM. The vibrational mode at 1842 cm^{-1} observed in the spectrum was attributed to the C=C stretching mode at ν_1. There appeared to be a cluster of four strong peaks in the experimental spectrum, as shown in Figure 6. However, an examination of the vibrational frequencies calculated at the B3LYP/6-31G(d) level (see Table 2) showed that the four peaks were, in fact, a cluster of six peaks that range in intensity from strong to very strong. Five of these peaks belonged to the CF stretching modes for the CF_3-group and CF_2=CF-groups. The absorption peak observed at 1195 cm^{-1} was assigned to the CO stretching mode. A comparison of the simulated spectrum, based on the B3LYP/6-31G(d) results, with the experimental spectrum showed that good agreement. Moreover, for the most part, the calculated vibrational frequencies and intensities were in good agreement with the experimental observed ones for $CF_3OCF=CF_2$.

4.3. Infrared Absorption Cross Section of $CF_3OCF=CF_2$

The examination of the assignments of the fundamental modes of $CF_3OCF=CF_2$ in the previous section has provided insight into the nature of the vibrations that contribute to absorption in the atmospheric window. The ν_2-ν_8 fundamental vibrations gave rise to quite strong absorption bands in the spectrum. As a result, these modes could be used as characteristic features to identify $CF_3OCF=CF_2$ in the atmosphere and, in conjunction with the absorption cross section, to estimate the Global Warming Potential of this molecule.

IR cross sections were determined on the basis of Beer's law using integrated absorption band coefficients. For each absorption band in the window of 1400-900 cm^{-1}, Beer's law plots were found to be linear. The integrated absorption cross sections for four intervals are summarized in Table 3. Radiation code used in this work requires the input of absorbance cross sections integrated over 30 wavelength intervals extending from 0 to 3000 cm^{-1}. Thus the absorbance cross sections are integrated into the 100 cm^{-1} bands listed in Table 3. Only the spectral range between 1100 cm^{-1} and 1400 cm^{-1} are significant for $CF_3OCF=CF_2$. The primary absorption in the 1400-900 cm^{-1} region was due to the CF and CO stretching modes for $CF_3OCF=CF_2$.

4.4. Atmospheric Lifetime for $CF_3OCF=CF_2$

The fast rate of $CF_3OCF=CF_2$ reaction with hydroxyl radicals renders $CF_3OCF=CF_2$ short-lived in the atmosphere. The model-

Table 3. Band Strengths for $CF_3OCF=CF_2$

Vibrational Mode	Integration Limits, cm^{-1}	Integrated Absorption Cross Section,[a] cm^2 $molecule^{-1}$ x 10^{17}
ν_8	1000-900	0.14 ± 0.1
ν_6–ν_7	1200-1100	7.82 ± 0.17
ν_5	1300-1200	10.04 ± 0.11
ν_2, ν_3, ν_4	1400-1300	6.98 ± 0.03

[a]Uncertainty is expressed as 2σ from the linear regression fit.

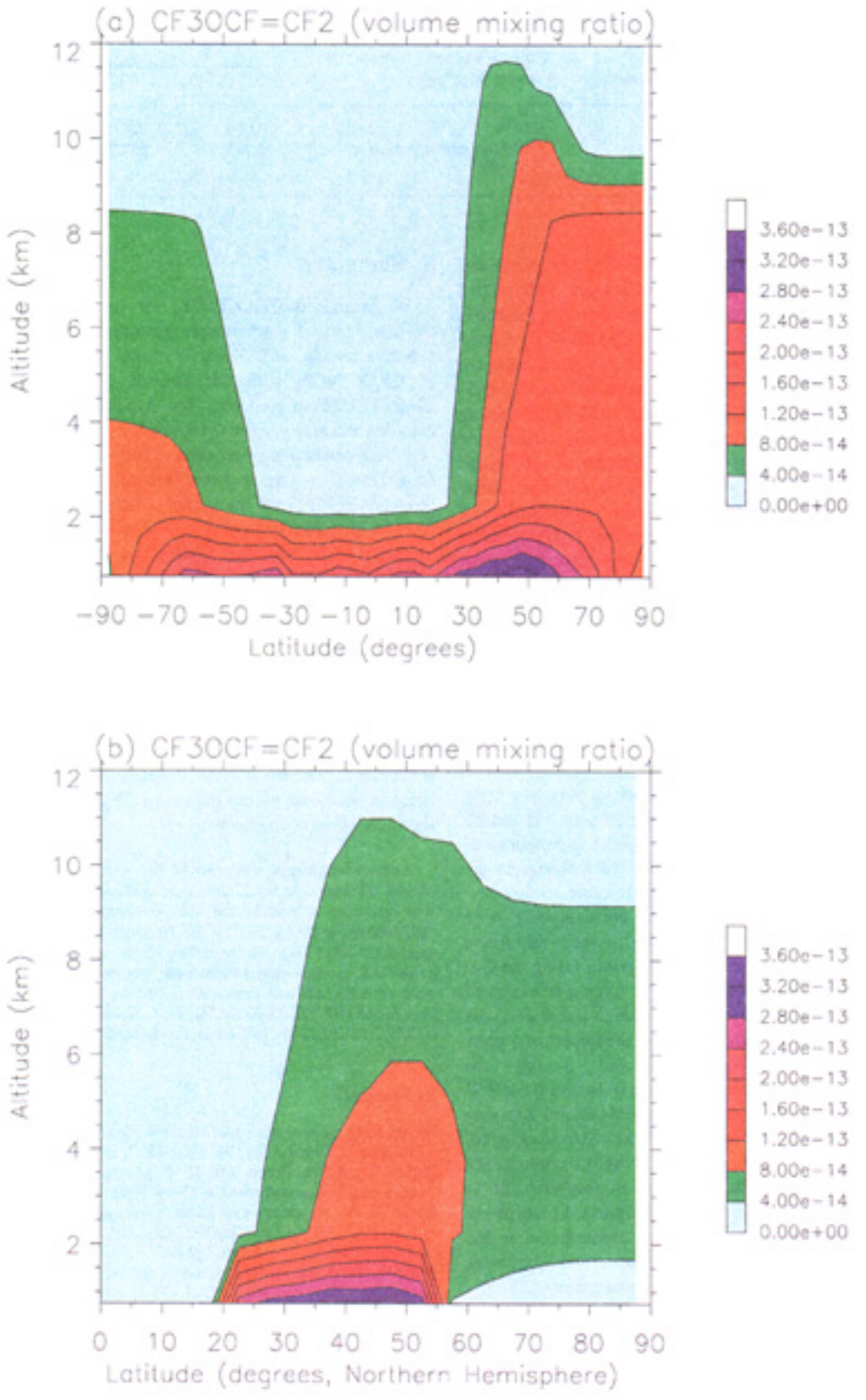

Plate 1. Atmospheric distribution of $CF_3OCF=CF_2$ from the 2-D chemical-transport-radiative model. (a) Global emission of $CF_3OCF=CF_2$ and (b) Northern hemisphere Mid-latitude emission of $CF_3OCF=CF_2$.

Table 4. Summary of Atmospheric Lifetime, Radiative Forcing, and GWPs for $CF_3OCF=CF_2$

Gas	Atmospheric Lifetime, years	Absolute Radiative Adjusted Forcing, W m^{-2} $ppbv^{-1}$	Global Warming Potentials, years		
			20	100	500
$CF_3OCF=CF_2$	0.010	0.0414	0.014	0.004	0.001
		0.0499 (constant vertical profile)	0.017	0.005	0.002

derived atmospheric lifetimes for $CF_3OCF=CF_2$ for global and midlatitude emission scenarios are ~0.010 years, and ~0.012 years, respectively. Lifetime estimated using the scaling method is 0.014 years. The atmospheric lifetime of $CF_3OCF=CF_2$ derived from the model is somewhat lower than that estimated using the scaling method. Notice that the rate constant for reaction (R1) was measured under total pressure of 1 torr (133 Pa) in present work, and this value would likely increase under atmospheric conditions since reaction (R1) involves addition of OH to the double bond. Thus $CF_3OCF=CF_2$ could have an even shorter atmospheric lifetime. Plates 1a and 1b give the vertical profiles of $CF_3OCF=CF_2$ derived from the two-dimensional (2-D) chemical transport model. Plate 1a shows the distribution for global emission of $CF_3OCF=CF_2$, while Plate 1b shows the distribution for emission only in the Northern Hemisphere midlatitudes. It is evident from both Plates that much of $CF_3OCF=CF_2$ is degraded within the troposphere.

4.5. Radiative Forcing and Global Warming Potentials for $CF_3OCF=CF_2$

The radiative forcing for $CF_3OCF=CF_2$ was derived for two different mixing ratio vertical profiles, a constant vertical profile, and the globally averaged vertical profile that was 2-D model-derived. Radiative forcing for a constant profile is evaluated as the change in forcing at the tropopause due to a change in the concentration from zero to 1 ppbv. The absolute cloudy-sky-adjusted forcing and instantaneous forcing are computed to be 0.0499 W m^{-2} $ppbv^{-1}$ and 0.0463 W m^{-2} $ppbv^{-1}$, respectively (these significant figures given for comparison purpose). Using the 2-D model-derived vertical profile, the radiative forcing is evaluated as the change in forcing at the tropopause due to a change in the surface concentration and rescaled to reflect the impact of 1 ppbv change. The absolute cloudy-sky-adjusted forcing and instantaneous forcing are determined to be 0.0414 and 0.0419 W m^{-2} $ppbv^{-1}$, respectively. The use of a model-derived decaying vertical profile results in a decrease in the radiative forcing by 10-15% as expected. The reduced radiative forcing is a consequence of reduced downwelling radiation in the troposphere due to smaller amount of $CF_3OCF=CF_2$ in the stratosphere. Stratospheric adjustment further reduces the forcing as stratospheric cooling due to reduced upwelling radiation from the troposphere dominates the warming due to increase in stratospheric absorption.

The Global Warming Potentials for $CF_3OCF=CF_2$ were evaluated using the model-erived atmospheric lifetime for global emission scenario and the adjusted radiative forcing for the time horizons corresponding to 20, 100, and 500 years of integration time and are given in Table 4. As mentioned earlier, CO_2 AGWPs were adopted from *WMO* [1998] for this calculation. The GWP for 100-year horizon for $CF_3OCF=CF_2$, 0.004, is insignificant in comparison with that of $CFCl_3$, 4000 [*WMO,* 1995]. This suggests that the use of $CF_3OCF=CF_2$ is unlikely to have any considerable effect on the climate.

5. Summary

We examined $CF_3OCF=CF_2$ for its reactivity toward OH radicals, infrared spectroscopic properties, atmospheric lifetime, radiative forcing, and Global Warming Potentials. The reaction of $CF_3OCF=CF_2$ with OH radicals produced both HF and $CF_3OCFC(O)F$ as products. The detailed reaction mechanism is complex and may involve the formation of an adduct intermediate or a four-center transition state. The Arrhenius expression for $CF_3OCF=CF_2$ + OH is determined to be $k_1 = (6.41\pm0.82)\times10^{-11}\exp[(-868\pm40)/T]$ cm^3 $molecule^{-1}$ s^{-1} in the temperature range of 253-348 K. The atmospheric lifetime of $CF_3OCF=CF_2$ is then estimated to be less than 5 days due to the OH attack. The calculated vibrational frequencies using ab initio molecular orbital calculations were in good agreement with FTIR experimental observation for the $CF_3OCF=CF_2$ molecule. Both C-O and C-F stretching modes in the $CF_3OCF=CF_2$ contribute to prominent absorption in the atmospheric window region. The adjusted radiative forcing for the $CF_3OCF=CF_2$ was calculated to be 0.041 W $m^{-2}ppbv^{-1}$. The Global Warming Potential for the $CF_3OCF=CF_2$ was predicted to be small (less than 0.01) due to the short atmospheric lifetime of this molecule. On the basis of this analysis we do not expect the use of $CF_3OCF=CF_2$ to lead to any significant impact on climate.

Acknowledgments. We would like to thank W. B. DeMore for helpful discussion in our kinetic data analysis. The experimental work was supported in part by the U.S. Environmental Protection Agency (X825967-01-0 EPA), and by the National Science Foundation (NSF grant ATM-9813331). The modeling studies were also supported in part by the U.S. Environmental Protection Agency (X829988-01 EPA). The work of A.K. Jain was supported in part by the U.S. National Science Foundation (NSF DMS-9711624), the U.S. Department of Energy (DOE DEFG02-96ER62284), and the Exxon Education Foundation.

References

Becke, A. D., A new mixing of Hatree-Fock and local density-functional theories, *J. Chem. Phys.*, *98*, 1372-1377, 1993.

Blukis, U., P. H. Kasai, and R. J. Myers, Microwave spectra and structure of dimethyl ether, *J. Chem. Phys.*, *38*, 2753-2760, 1963.

Boulet G. A., An electron diffraction investigation of the structures of CH_3COCl, CF_3COCl, CH_3COF, CF_3COF, CF_3COCF_3, Ph.D. thesis, Univ. of Mich., Ann Arbor, 1964.

Briegleb, B., Longwave band model for thermal radiation in climate studies, *J. Geophys. Res.*, *97*, 11,475-11,485, 1992a.

Briegleb, B., Delta-Eddington Approximation for solar radiation in the NCAR community climate model, *J. Geophys. Res.*, *97*, 7603-7612, 1992b.

Brown, R.L., Tubular flow reactions with first-order kinetics, *J. Res. Natl. Bur. Stand. U.S. 83*, 1-8, 1978.

Chang, J.S., and F. Kaufman, Kinetics of the reactions of hydroxyl radicals with some halocarbons: $CHFCl_2$, CHF_2Cl, CH_3CCl_3, C_2HCl_3, and C_2Cl_4, *J. Chem. Phys.*, *66*, 4989-4994, 1977.

Christidis, N., M. D. Hurley, S. Pinnock, K. P. Shine, and T. J. Wallington, Radiative forcing of climate change by CFC-11 and possible CFC replacements, *J. Geophys. Res.*, *102*, 19,597-19,609, 1997.

DeMore, W.B., S.P. Sander, D.H. Golden, R.F. Hampson, M.J. Kurylo, C.J. Howard, A.R. Ravishankara, C.E. Kolb, and M.J. Molina, Chemical kinetics and photochemical data for use in stratospheric modeling, Evaluation number 12, *JPL Publ., 97-4*, 1997.

Frisch, M. J., et al., GAUSSIAN 94, Revision D.2, GAUSSIAN, Inc., Pittsburgh, Pa., 1995.

Good, D. A., J. S. Francisco, A. K. Jain, and D. J. Wuebbles, Lifetimes and global warming potentials for dimethyl ether and for fluorinated ethers: CH_3OCF_3 (E143a), CHF_2OCHF_2 (E134), CHF_2OCF_3 (E125), *J. Geophys. Res., 103*, 28,181-28,186, 1998.

Howard, C.J., Kinetic measurements using flow tubes, *J. Phys. Chem., 83*, 3-9, 1979.

Intergovernmental Panel on Climate Change (IPCC), *Climate Change, The IPCC Scientific Assessment*, edited by J. T. Houghton, G. J. Jenkins, and J. J. Ephraums, Cambridge Univ. Press, New York, 1990.

Intergovernmental Panel on Climate Change (IPCC), *Climate Change, 1992: The Supplementary Report to the IPCC Scientific Assessment*, edited by J.T. Houghton, B.A. Callader, S.K. Varney, Cambridge Univ. Press, New York, 1992.

Intergovernmental Panel on Climate Change (IPCC), *Climate Change 1994: Radiative Forcing of Climate Change and an Evaluation of the IPCC IS92 Emission Scenarios*, edited by J. T. Houghton et al., Cambridge Univ. Press, Cambridge, New York, 1995.

Intergovernmental Panel on Climate Change (IPCC), *Climate Change 1995: The Science of Climate Change*, edited by J. T. Houghton et al., Cambridge Univ. Press, New York, 1996.

Kiehl, J. T., and B. Briegleb, The relative role of sulfate aerosols and greenhouse gases in climate forcing, *Science, 260*, 311-314, 1993.

Lee, C., W. Yang, and R. G. Parr, Development of the Colle-Salvetti

Pinnock, S., M.D. Hurley, K.P. Shine, T.J. Wallington, and T.J. Smyth, Radiative forcing of climate by hydrochlorofluorocarbons and hydrofluorocarbons, *J. Geophys. Res., 100*, 23,227-23,238, 1995.

Prather, M.J. and C.M. Spivakovsky, Tropospheric OH and the lifetimes of hydrofluorocarbons (HCFCs), *J. Geophys. Res.* 95, 18723-18729, 1990.

Prinn, R., R.F. Weiss, B.R. Miller, J. Huang, F. Alyea, D.M. Cunnold, P.J. Fraser, D. Hartley, and P. Simmonds, Atmospheric trends and lifetime of trichloroethane and global average of hydroxyl radical concentrations based on 1978-1994 ALE/GAGE measurements, *Science, 269*, 187-192, 1995.

Rahmes, T.F., A.H. Omar, and D.J. Wuebbles, Atmospheric distributions of soot particles by current and future aircraft fleets and resulting radiative forcing on climate, *J. Geophys. Res.*, in press, 1999.

Ravishankara, A. R., J.M. Nlocovich, R. L. Thompson, and F. P. Tully, Kinetic study of the reaction of OH with H_2 and D_2 from 250 to 1050 K, *J. Phys. Chem., 85*, 2498-2503, 1981.

Ravishankara, A.R., S. Solomon, A.A. Turnipseed, and R.F. Warren, Atmospheric lifetimes of long-lived halogenated species, *Science, 259*, 194-199, 1993.

Rothman, L.S., R.R. Gamache, A. Goldman, L.R. Brown, R.A. Toth, H.M. Pickett, R.L. Poynter, J.M. Fland, C. Camy-Peyret, A. Barbe, N. Husson, C.P. Rinsland, and M.A. Smith, The HITRAN database: 1986 edition, *Appl. Opt, 26*, 4058-4097, 1987.

Schlegel, H. B., Optimization of equilibrium geometries and transition structures, *J. Comput. Chem., 3*, 214-218, 1982.

Wine, P. H., N. M. Kreutter, and A. R. Ravishankara, Flash photolysis-resonance fluorescence kinetics study of the reaction OH + NO_2 + M $\rightarrow$ HNO_3 + M, *J. Phys. Chem., 83*, 3191-3195, 1979.

World Meteorological Organization (WMO), Scientific assessment of

CH_4, and C_2H_6, *J. Phys. Chem., 99*, 13,445-13,451, 1995.

Li, Z., R.R. Freidl, and S.P. Sander, Kinetics of the HO_2 + BrO reaction over the temperature range 233-348 K, *J. Chem. Soc. Faraday Trans., 93*, 2683-2691, 1997.

McIlroy, A., and F. P. Tully, Kinetic study of OH reactions with perfluoropropene and perfluorobenzene, *J. Phys. Chem., 97*, 610-614, 1993.

Mellouki, A., S. Teton, and G. Le Bras, Rate constant for the reaction of OH radical with HFC-365mfc ($CF_3CH_2CF_2CH_3$), *Geophys. Res. Lett., 22*, 389-392, 1995.

Orkin, V.L., R.E. Huie, and M.J. Kurylo, Rate constant for the reactions of OH with HFC-245cb ($CH_3CF_2CF_3$) and some fluoroalkenes (CH_2CHCF_3, CH_2CFCF_3, CF_2CFCF_3, and CF2CF2), *J. Phys. Chem. A, 101*, 9118-9124, 1997.

Patten, K.O., P.S. Connel, D.E. Kinnison, D.J. Wuebbles, L. Froidevaux, and T.G. Slanger, Effect of vibrationally excited oxygen on ozone production in the stratosphere, *J. Geophys. Res., 99*, 1211-1224, 1994.

Perry, R.A., R. Atkinson, and J.N. Pitts Jr., Rate constant for the reaction of OH radicals with dimethyl ether and vinyl methyl ether over the temperature range 299-427 K, *J. Chem. Phys., 67*, 611-614, 1977.

Yoshida, Y., Japan's research on alternative etching gases, paper presented at Global Semiconductor Industry Conference on PFC Emission Control, sponsored by U.S. EPA, Monterey, Ca., 1998.

J. S. Francisco, D. A. Good, and J. C. Hansen, Department of Chemistry and Departemt of Earth and Atmospheric Sciences, Purdue University, West Lafayette, IN 47907-1393. (jfrancis@cv3.chem.purdue.edu; goodda@aurora.eas.purdue.edu; jchansen@purdue.edu.)

A.K. Jain, G.R. Jeong, Z. Li, V. Naik, Z. Tao, and D. J. Wuebbles, Department of Atmospheric Sciences, University of Illinois at Urbana-Champaign, Urbana, IL 61801. (jain@atmos.uiuc.edu; gill@atmos.uiuc.edu; zli@atmos.uiuc.edu; vnaik@atmos.uiuc.edu; zhining@atmos.uiuc.edu; wuebbles@atmos.uiuc.edu.)

(Received March 4, 1999; revised August 31, 1999; accepted September 3, 1999.)